Title
In vivo blood flow imaging by a swept laser source based Fourier domain optical Doppler tomography

Journal
Optics Express, 13(19)

ISSN
1094-4087

Authors
Zhang, Jun
Chen, Zhongping

Publication Date
2005

DOI
10.1364/OPEX.13.007449

Peer reviewed

In vivo blood flow imaging by a swept laser source based Fourier domain optical Doppler tomography

Jun Zhang, Zhongping Chen

Beckman Laser Institute and the Center for Biomedical Engineering
University of California, Irvine, California 92612
junzhang@uci.edu, z2chen@uci.edu

Abstract: A swept source based Fourier domain optical Doppler tomography (FDODT) system was developed. The technique is based on a phase-resolved method where phase information was retrieved from the reconstructed complex fringe signals. The aliasing effects and artifacts caused by lateral scanning and sample movement were removed with a signal processing technique. The standard deviation of the phase shift of the system was reduced from 49 to 1.8 degrees with the signal processing method employed. Structural, Doppler and Doppler variance images of fluid flow through glass channels were quantified, and blood flow through vessels of chick chorioallantoic membrane (CAM) was demonstrated in vivo.

OCIS codes: (170.4500) Optical coherence tomography; (070.2590) Fourier transforms; (170.3340) Laser Doppler velocimetry;

References and links

1. D. Huang, E. A. Swanson, C. P. Lin, J. S. Schuman, W. G. Stinson, W. Chang, M. R. Hee, T. Flotte, K. Gregory, C. A. Puliafito, J. G. Fujimoto, "Optical coherence tomography," Science **254**, 1178-1181 (1991).
2. A. F. Fercher, C. K. Hitzenberger, G. Kamp, and S. Y. Elzaiat, "Measurement of intraocular distances by backscattering spectral interferometry," Opt. Commun. **117**, 43-48 (1995).
3. G. Hausler and M. W. Linduer, "Coherence radar and spectral radar-new tools for dermatological diagnosis," J. Biomed. Opt. **3**, 21-31 (1998).
4. R. A. Leitgeb, C. K. Hitzenberger, and A. F. Fercher, "Performance of fourier domain vs. time domain optical coherence tomography," Opt. Express **11**, 889-894 (2003). http://www.opticsexpress.org/abstract.cfm?URI=OPEX-11-8-889.
5. M. Wojtkowski, V. J. Srinivasan, T. H. Ko, J. G. Fujimoto, A. Kowalczyk, and J. S. Duker, "Ultrahigh-resolution, high-speed, Fourier domain optical coherence tomography and methods for dispersion compensation," Opt. Express **12**, 2404-2422 (2004). http://www.opticsexpress.org/abstract.cfm?URI=OPEX-12-11-2404
6. B. Cense, N. A. Nassif, T. C. Chen, M. C. Pierce, S. Yun, B. H. Park, B. E. Bouma, G. J. Tearney, and J. F. de Boer, "Ultrahigh-resolution high-speed retinal imaging using spectral-domain optical coherence tomography," Opt. Express **12**, 2435-2447 (2004). http://www.opticsexpress.org/abstract.cfm?URI=OPEX-12-11-2435
7. S. Jiao, R. Knighton, X. Huang, G. Gregori, and C. A. Puliafito, "Simultaneous acquisition of sectional and fundus ophthalmic images with spectral-domain optical coherence tomography," Opt. Express **13**, 444-452 (2005). http://www.opticsexpress.org/abstract.cfm?URI=OPEX-13-2-444
8. M. A. Choma, M. V. Sarunic, C. H. Yang, and J. A. Izatt, "Sensitivity advantage of swept source and Fourier domain optical coherence tomography," Opt. Express **11**, 2183-2189 (2003). http://www.opticsexpress.org/abstract.cfm?URI=OPEX-11-18-2183
9. S. H. Yun, G. J. Tearney, J. F. de Boer, N. Iftimia, and B. E. Bouma, "High-speed optical frequency-domain imaging," Opt. Express **11**, 2953-2963 (2003). http://www.opticsexpress.org/abstract.cfm?URI=OPEX-11-22-2953
10. S. R. Chinn, E. A. Swanson, and J. G. Fujimoto, "Optical coherence tomography using a frequency-tunable optical source," Opt. Lett. **22**, 340-342 (1997).

#8177 - $15.00 USD Received 15 July 2005; revised 2 September 2005; accepted 6 September 2005

11. S. H. Yun, C. Boudoux, G. J. Tearney, and B. E. Bouma, "High-speed wavelength-swept semiconductor laser with a polygon-scanner-based wavelength filter," Opt. Lett. **28**, 1981-1983 (2003).
12. R. Huber, M. Wojtkowski, K. Taira, J. G. Fujimoto, and K. Hsu, "Amplified, frequency swept lasers for frequency domain reflectometry and OCT imaging: design and scaling principles," Opt. Express **13**, 3513-3528 (2005). http://www.opticsexpress.org/abstract.cfm?URI=OPEX-13-9-3513
13. J. Zhang, J. S. Nelson, and Z. P. Chen, "Removal of a mirror image and enhancement of the signal-to-noise ratio in Fourier-domain optical coherence tomography using an electro-optic phase modulator," Opt. Lett. **30**, 147-149 (2005).
14. R. A. Leitgeb, M. Wojtkowski, A. Kowalczyk, C. K. Hitzenberger, M. Sticker, and A. F. Fercher, "Spectral measurement of absorption by spectroscopic frequency-domain optical coherence tomography," Opt. Lett. **25**, 820-822 (2000).
15. R. A. Leitgeb, L. Schmetterer, C. K. Hitzenberger, A. F. Fercher, F. Berisha, M. Wojtkowski, and T.Bajraszewski, "Real-time measurement of in vitro flow by Fourier-domain color Doppler optical coherence tomography," Opt. Lett. **29**, 171-173 (2004).
16. B. R. White, M. C. Pierce, N. Nassif, B. Cense, B. H. Park, G. J. Tearney, B. E. Bouma, T. C. Chen, and J. F. de Boer, "In vivo dynamic human retinal blood flow imaging using ultra-high-speed spectral domain optical coherence tomography," Opt. Express **11**, 3490-3497 (2003). http://www.opticsexpress.org/abstract.cfm?URI=OPEX-11-25-3490
17. B. H. Park, M. C. Pierce, B. Cense, S. Yun, M. Mujat, G. J. Tearney, B. E. Bouma, and J. F. de Boer, "Real-time fiber-based multi-functional spectral-domain optical coherence tomography at 1.3 μm," Opt. Express **13**, 3931-3944 (2005). http://www.opticsexpress.org/abstract.cfm?URI=OPEX-13-11-3931
18. Y.Yasuno, S.Makita, Y.Sutoh, M.Itoh, and T.Yatagai, "Birefringence imaging of human skin by polarization-sensitive spectral interferometric optical coherence tomography," Opt. Lett. **27**, 1803-1805 (2002).
19. J. Zhang, W. Jung, J. S. Nelson, and Z. Chen, "Full range polarization-sensitive Fourier domain optical coherence tomography," Opt. Express **12**, 6033-6039 (2004). http://www.opticsexpress.org/abstract.cfm?URI=OPEX-12-24-6033
20. Y. H. Zhao, Z. P. Chen, C. Saxer, Q. M. Shen, S. H. Xiang, J. F. de Boer, J. S. Nelson, "Doppler standard deviation imaging for clinical monitoring of in vivo human skin blood flow," Opt. Lett. **25**, 1358-1360 (2000).
21. Y. Zhao, Z. Chen, C. Saxer, S. Xiang, J. F. de Boer, and J. S. Nelson, "Phase Resolved Optical Coherence Tomography and Optical Doppler Tomography for Imaging blood flow in human skin with fast scanning speed and high velocity sensitivity," Opt. Lett. **25**, 114-116 (2000).
22. S. H. Yun, G. J. Tearney, J. F. de Boer, and B. E. Bouma, "Motion artifacts in optical coherence tomography with frequency-domain ranging," Opt. Express **12**, 2977-2998 (2004). http://www.opticsexpress.org/abstract.cfm?URI=OPEX-12-13-2977.

1. Introduction

Optical coherence tomography (OCT) is a noninvasive, noncontact imaging modality that uses coherent gating to obtain high-resolution cross-sectional images of tissue microstructure [1]. Compared with conventional time domain OCT (TDOCT), which is based on a scanning optical delay line, Fourier domain OCT (FDOCT) can obtain higher sensitivity and imaging speed [2-13]. Two methods have been developed to employ the Fourier domain technique: FDOCT using a spectrometer with a multi-channel analyzer [2-7] and FDOCT using a rapidly swept laser source [8-13]. In addition to the morphological structural image, FDOCT can also provide functional information of tissue physiology such as absorption [14], blood flow velocity [15-17] and birefringence [17-19]. However, most reported FD functional OCT systems are based on a spectrometer, which requires a high speed line-scan camera. Although high speed line-scan cameras with large arrays are readily available at 800 nm, linear scan cameras with high sensitivity at 1300 nm have a limited pixel number and are very expensive. In addition, the obscure object structure and phase error due to the mirror image generated by the Fourier transform and the low frequency autocorrelation noises originating from the reflected terms from the reference mirror and sample compromise the reconstruction of complex fringe signals. In a spectrometer based FDOCT system, removal of the mirror image and autocorrelation term requires multiple A-line data to process, which reduces imaging speed. Our recent work shows that complete removal of the autocorrelation noise and mirror image using an electro-optic (EO) phase modulator can achieve the full range complex signal instantaneously in swept source based FDOCT system [13,19].

#8177 - $15.00 USD Received 15 July 2005; revised 2 September 2005; accepted 6 September 2005

In this paper, the swept source based FDOCT system was developed to acquire blood flow velocity of tissue. A phase-resolved signal processing method was adopted to acquire the velocity and standard deviation images by processing the analytical interference complex fringe signals.

2. Experimental setup and signal processing

The schematic diagram of the fiber based Fourier domain optical Doppler tomography (FDODT) system is shown in Fig. 1. The output light from a swept laser source (Micron Optics, Inc.) at 1.31 μm with a FWHM bandwidth of 85 nm, output power of 5 mW and instantaneous linewidth of 0.1 nm was split into reference and sample arms by a 2 × 2 coupler. The laser source was driven by a 2 KHz sinusoidal signal. In the reference arm, an EO phase modulator (JDS Uniphase) was used to generate a stable carrier frequency of 2 MHz for elimination of the mirror image and low frequency noise. The EO phase modulator was driven by a ramp waveform with 40 MHz sampling rate. The corresponding double pass distance shift was about 5 mm which is sufficient to separate the positive and negative terms as well as the low frequency terms. To match dispersion caused by the EO phase modulator, an optical setup similar to a rapid scanning optical delay (RSOD) line with a stationary mirror was adopted which can compensate the second order group velocity dispersion. Calculation showed the third and higher order dispersion can be neglected in our system. The reference power was attenuated by an adjustable neutral density attenuator for maximum sensitivity. 5% of the laser output was split and propagated through a 100 GHz fiber Fabry-Perot (FFP) interferometer (Micron Optics) to generate comb signals for dynamic calibration of the swept wavenumber function that is essential for rigorous conversion from time to wavenumber space. In the detection arm, the signal from the photodetectors was converted by a 12 bit data acquisition board sampling at 10 MHz. The complex analytical depth encoded signal was converted from the time fringe signal by the digital approach shown in the following block diagram:

$$\Gamma(t) \rightarrow \boxed{FFT} \rightarrow \boxed{\times H(\nu)} \rightarrow \boxed{\text{Bandpass Filter}} \rightarrow \boxed{\text{Demodulation}} \rightarrow \boxed{FFT^{-1}}$$

$$\rightarrow \tilde{\Gamma}(t) \rightarrow \boxed{\text{Spectra Calibration}} \rightarrow \tilde{I}(k) \rightarrow \boxed{FFT} \rightarrow \tilde{S}(z)$$

where FFT denotes the fast Fourier transform, × is a multiplying symbol, $H(\nu)$ is the Heaviside function given by:

$$H(\nu) = \begin{cases} 0 & \nu < 0 \\ 1 & \nu \geq 0 \end{cases} \tag{1}$$

and FFT^{-1} denotes the inverse fast Fourier transform. The time fringe signal $\Gamma(t)$ is first transformed from time to frequency space by FFT. Multiplication of the Heaviside function and the process of band pass filtering select the positive term of the Fourier transformed interference signal. The subsequent demodulation step removes the carrier frequency. The frequency fringe signal is then converted back to time space by FFT^{-1}. The spectra calibration determines the function of $k(t)$ before conversion from time to wavenumber space. The last FFT performed in k space retrieves the complex depth encoded fringe signal $\tilde{S}(z) = A(z)e^{i\phi(z)}$ which contains both the amplitude $A(z)$ and phase $\phi(z)$ terms. From the amplitude information of $\tilde{S}(z)$, the structure image can be acquired. Doppler processing can be implemented from the phase term of $\tilde{S}(z)$ to visualize blood flow. The Doppler frequency shift and the standard deviation of the Doppler frequency spectrum are determined from the phase shift between sequential A-line scans. To increase the signal to noise ratio (SNR), five

#8177 - $15.00 USD Received 15 July 2005; revised 2 September 2005; accepted 6 September 2005

sequential A-line scans are averaged which allows a real time Doppler tomogram rate of around 1 frame per second.

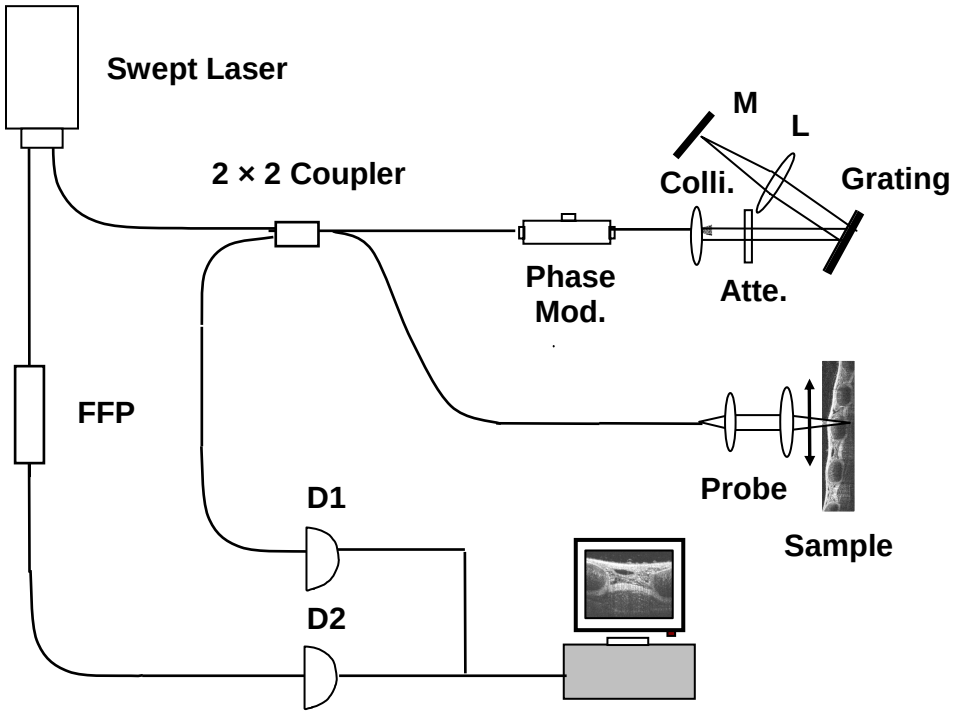

Fig. 1. Schematic of the FDODT system. Phase Mod.: phase modulator; Colli.: collimator; Atte.: adjustable neutral density attenuator; M: mirror; L: Lens; FFP: 100 GHz fiber Fabry-Perot interferometer; D1, D2: photodetectors.

The Doppler shift is obtained by [20]:

$$f_D = \frac{\Delta\phi(z)}{2\pi T} = \frac{1}{2\pi T}\tan^{-1}\left(\frac{\mathrm{Im}(\sum_{j=1}^{N}\tilde{S}_{jT}(z)\cdot\tilde{S}^{*}_{(j+1)T}(z))}{\mathrm{Re}(\sum_{j=1}^{N}\tilde{S}_{jT}(z)\cdot\tilde{S}^{*}_{(j+1)T}(z))}\right) \quad (2)$$

where N is the number of A-lines used for averaging; T is the time interval between successive A scans; and $\tilde{S}_{jT}(z)$ and $\tilde{S}^{*}_{jT}(z)$ are the complex signal at axial pixel z, corresponding to the jth A-scan and its conjugate, respectively. T determines the Doppler frequency shift range, namely, the velocity dynamic range because $\Delta\varphi(z)$ can only be correctly traced between $-\pi$ and π. In FDODT, a large velocity dynamical range is possible since A-scan can be much faster using Fourier domain method. Therefore, FDODT is capable of imaging and quantifying ultra-fast flow dynamics. In addition to the local velocity information, FDODT system gives the variance of local velocity, which is given by [20]:

#8177 - $15.00 USD Received 15 July 2005; revised 2 September 2005; accepted 6 September 2005

$$\sigma^2 = \frac{1}{T^2}\left\{1 - \frac{\left|\sum_{j=1}^{N} \tilde{S}_{jT}(z) \cdot \tilde{S}^{*}_{(j+1)T}(z)\right|}{\sum_{j=1}^{N} \tilde{S}_{jT}(z) \cdot \tilde{S}^{*}_{jT}(z)}\right\} \quad (3)$$

The value of σ^2 depends on the flow velocity distribution. Variations of flow velocity broaden the Doppler frequency spectrum and result in a larger σ^2. Thus, the Doppler variance image can be an indicator of flow variations and can be used to study flow turbulences.

3. Experimental results

Phase-resolved technique allows high sensitivity blood flow measurement [20,21]. However, this method also suffers from the phase error due to environmental disturbances, such as table oscillation and fiber movement during sampling probe scanning. Moreover, compared with a spectrometer based FDOCT system, the repeatability of the wavelength scanning in a swept source based FDOCT system is difficult to maintain, and additional phase error will be induced. The minimum detectable velocity is dependent on the phase error in the system. To evaluate the phase stability of the system, stationary microscope cover glasses with thickness of 150 μm were used as the samples. For every lateral position, five sequential A-line scans were performed to obtain the phase shift. 4000 A scans were averaged to determine the phase difference between adjacent A-lines of the light reflected from the second surface. The phase variations are demonstrated in Fig. 2(a) showing an average phase shift of 4.88° and a standard deviation of 48.75°. The measurement error is due to the large background noise. The background Doppler shift can be removed if we can designate a static object as a reference for the initial phase in each A-line scan. Taking the first surface of the glass as the phase reference, the background noise is removed efficiently. Figure 2(b) shows the corrected phase variation with an average phase shift of - 0.12° and the standard deviation of 1.77°. There is another possible phase error in a swept source based FDOCT system which comes from the fluctuation of initial wavenumber between sequential A scans. This phase error cannot be compensated by use of the phase reference technique since the induced phase error increases linearly with the depth. Synchronizing wavelength sweeping and the data acquisition using a portion of the output light through a fiber brag grating (FBG) to trigger the data acquisition can reduce this phase error. However, even though a narrow linewidth FBG was used, the phase error still exists due to the limited sampling interval, and to reduce this phase error, a high sampling frequency data acquisition board is required. In our system, the number of data points for each A-line is 1600. The corresponding acquisition time is 0.16 ms during which the wavelength of 85 nm is scanned. The fluctuation of wavenumber in one sampling interval is 190 m^{-1}. At depth of 150 μm, maximum phase error is about 1.6°. Considering a depth range of 2 mm and the Gaussian shape distribution of phase shift, the standard deviation of the phase error is about 4° which can be neglected in our experiment.

#8177 - $15.00 USD Received 15 July 2005; revised 2 September 2005; accepted 6 September 2005

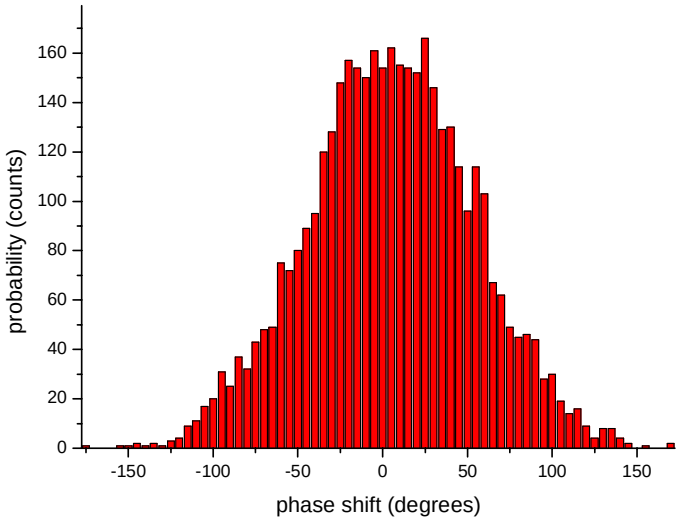

(a)

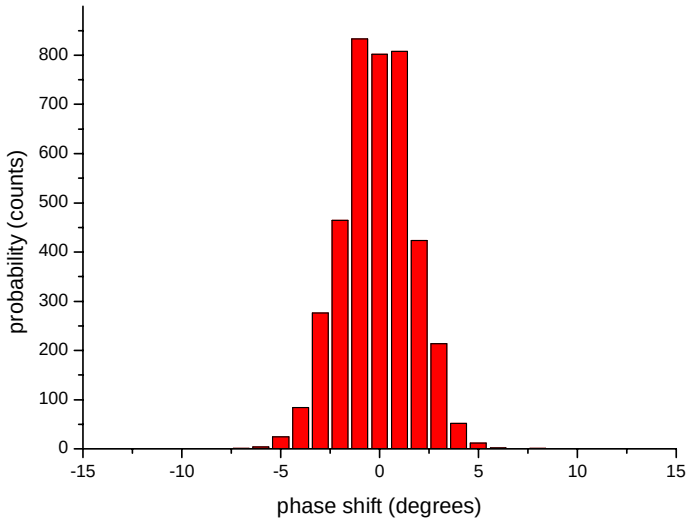

(b)

Fig. 2. Probability distribution of measured phase difference from the second surface of a stationary microscope cover glass without (a) and with (b) background noise reduction.

Figure 3 shows the structural, velocity and Doppler variance images of a scattering fluid flow through a glass channel. A polystyrene bead solution (mean diameter: 0.3 μm, volume concentration: 0.26%) was used as working fluid. The fluid was driven through a glass channel (outer diameter: 700 μm; inner diameter: 500 μm) by a syringe pump. The fluid was pumped into the glass channel at a rate of 20 μl/min, corresponding to an average flow velocity of 1.70 mm/s within the glass channel. The surface layer with thickness of 100 μm was taken as the reference for the initial phase and zero background. Fig. 3a shows the structural image of the glass channel with polystyrene beads. Fig. 3b is the velocity image of

#8177 - $15.00 USD Received 15 July 2005; revised 2 September 2005; accepted 6 September 2005

the flowing fluid. The Doppler angle was set to 84°. The velocity was color-coded into red and blue to represent two opposite directions. The presence of different velocities (property of pressure driven flow) within the glass channel was observed. Figure 3(c) shows the normalized Doppler variance image that gives the variation of the fluid velocity distribution. The velocity profile in the axial direction in the center of the channel is shown in Fig. 3(d). The profile fits well the parabolic shape which reflects the property of pressure driven flow as expected. To show the blood flow dynamics more clearly, the structural, velocity and Doppler variance images are shown in three-dimensional format in Fig. 4.

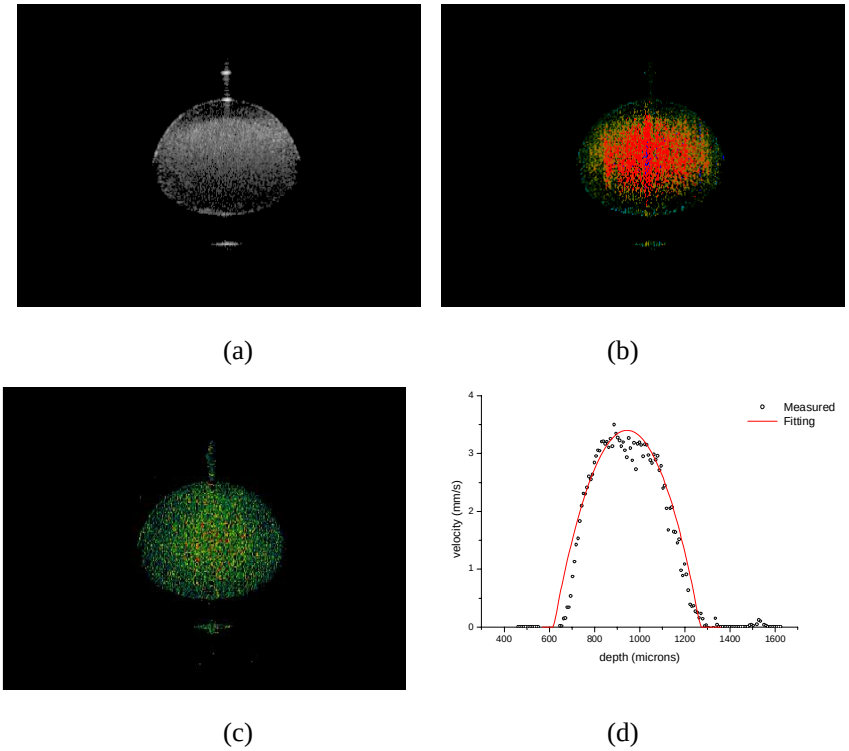

Fig. 3. Structural (a),velocity (b) and Doppler variance (c) images of a fluid flow. (d) The velocity profile in the axial direction in the center of the channel. Channel dimension: 0.5 mm.

To illustrate the performance of the system in biological tissues, the chick chorioallantoic membrane (CAM) was imaged. The CAM is a well established model for studying the microvasculature and has been used extensively to investigate the effects of vasoactive drugs as well as optical and thermal processes in blood vessels. The structural and velocity images of a 6 days old CAM are shown in Fig. 5. The imaged area is 4 × 3 mm with the zero distance difference set in the center of the depth scale. The surface layer with thickness of 100 μm was taken as the reference for the initial phase and zero background. The blood vessel was evident in the velocity image. The velocity profile in the axial direction in the center of the vessel is shown in Fig. 5c. Axial motion artifacts in FDOCT can give rise to depth error, reduction in spatial resolution and SNR degradation [22]. However, these effects can be neglected in the experiment since motion of the 6 days old CAM is quite weak.

#8177 - $15.00 USD Received 15 July 2005; revised 2 September 2005; accepted 6 September 2005

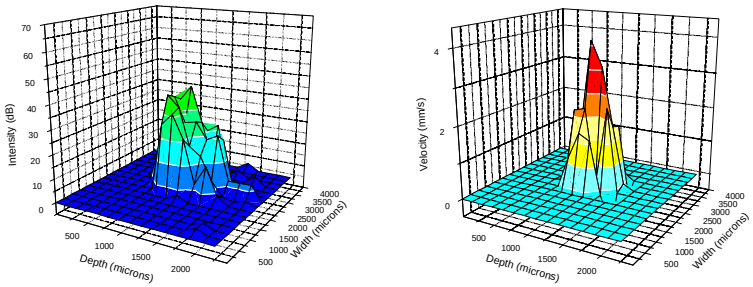

(a) (b)

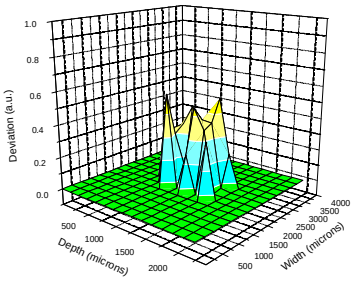

(c)

Fig. 4. Three-dimensional structural (a),velocity (b) and Doppler variance (c) images of a fluid flow through a glass channel.

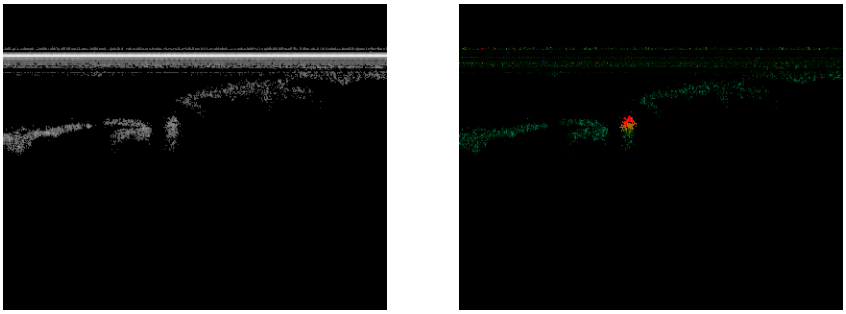

(a) (b)

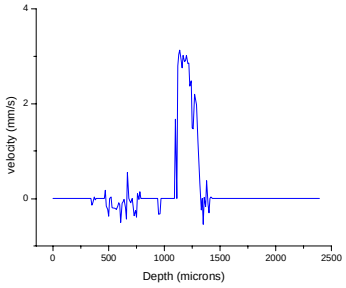

(c)

Fig. 5. Structural (a) and velocity (b) images of the blood flow in chick chorioallantoic membrane. (c) The velocity profile in the axial direction in the center of the vessel.

#8177 - $15.00 USD Received 15 July 2005; revised 2 September 2005; accepted 6 September 2005

4. Summary

A phase-resolved swept source based FDODT system was developed. The aliasing effects and artifacts caused by lateral scanning and sample movement were removed with a signal processing technique. Structural, Doppler and Doppler variance images of fluid flow through glass channels were quantified, and blood flow through vessels of chick chorioallantoic membrane (CAM) was demonstrated.

Acknowledgments

We acknowledge the valuable contributions of Ku Youn Baik, Nzola Magalhaes, and Chung-Ho Sun. This work was supported by research grants from the National Science Foundation (BES-86924), National Institutes of Health (EB-00293 and EB-002495, NCI-91717, RR-01192), Air Force Office of Scientific Research (FA9550-04-1-0101), and the Beckman Laser Institute Endowment.

#8177 - $15.00 USD Received 15 July 2005; revised 2 September 2005; accepted 6 September 2005